Optical properties of Rydberg excitons and polaritons

Sylwia Zielińska-Raczyńska, Gerard Czajkowski, and David Ziemkiewicz*
Institute of Mathematics and Physics, UTP University of Science and Technology, and Al. Kaliskiego 7, 85-789 Bydgoszcz, Poland
(Received 9 December 2015; revised manuscript received 24 January 2016; published 26 February 2016)

We show how to compute the optical functions when Rydberg excitons appear, including the effect of the coherence between the electron-hole pair and the electromagnetic field. We use the real density matrix approach (RDMA), which, combined with the Green's function method, enables one to derive analytical expressions for the optical functions. Choosing the susceptibility, we performed numerical calculations appropriate to a Cu_20 crystal, being a semiconductor with an indirect gap. The effect of the coherence is displayed in the line shape. We also examine in detail and explain the dependence of the oscillator strength and the resonance placement on the state number. We report good agreement with recently published experimental data. We also show that the presented method can be applied to semiconductors with a direct gap.

DOI: 10.1103/PhysRevB.93.075206

I. INTRODUCTION

Since the 1980s Rydberg atoms, in which the valence electron is in a state of high principal quantum number $n \gg 1$, have been extensively studied. They have exaggerated atomic properties, including dipole-dipole interactions that scale as $\sim n^4$ and radiative lifetimes proportional to n^2. Another important property of the Rydberg states is the large orbital radius, and hence dipole moment $\sim n^2$. The natural consequence of the large dipole moment featured by the Rydberg atoms is the large interaction between two of them—one is able to observe dipole-dipole interactions between atoms on the micro scale. Another consequence of the incredibly large dipole moment is an exaggerated response to external fields [1]. Due to a small admixing of the Rydberg state with the ground one, the atoms experience long-range and large interactions while keeping a long lifetime in a quantum superposition, which is very useful for creating qubits, so Rydberg atoms are well suited to applications in quantum information processing. The idea of using dipolar Rydberg interactions to implement the Rydberg blockade is based on the fact that in an ensemble of atoms with long-range dipolar interactions between them, only one atom can be excited at given time. This "dipole blockade" has now been observed for two single atoms positioned at macroscopic distances [2]. Rydberg interaction between distanced atoms is used to implement one- or two-qubit quantum gates of high fidelity [3]. Coupling of Rydberg states results in the dc Kerr effect, which is 6 orders of magnitude greater than in the conventional Kerr effect. This result has great impact on development of high-precision electric field sensors and other nonlinear optical devices [4]. Rydberg atoms are also applied in single-microwave-photon counters, which is especially promising in high-precision measurements in quantum optics [5]. On this wide background of potential applications established in quantum optics and atomic physics, the demonstration of giant Rydberg excitons in copper oxide [6,7] is a great step toward studies that are out of the reach in atomic physics, e.g., Rydberg excitons, due to their smaller energies, need for lower magnetic fields to mimic hydrogen atoms in white-dwarf stars [8], or they are promising candidates for creating Bose-Einstein condensate in solids [9].

The phenomenon of excitons and their consequences on the optical spectra of semiconductors, intensively studied over the decades, obtained a new impulse when the so-called Rydberg excitons were detected in a natural crystal of copper oxide found at the Tsumeb mine in Namibia [6,7]. In the simplest picture the exciton (we have in mind the so-called Wannier exciton) is modeled as a hydrogenlike atom, composed from the electron and the hole, interacting via the Coulomb potential screened by the semiconductor dielectric constant. The materials, where Wannier excitons occur, show optical spectra where the transition states, related to the principal quantum number n, are observed. In most previously studied materials, such as, for example, GaAs, only a few excited excitonic states ($n = 1,2,3$) were detected, which was caused by the small excitonic binding energy (in the order of a few meV, as in GaAs) and dissipative processes. Therefore the discovery reported in Ref. [7], where the analysis of the spectra revealed spectral absorption lines associated with the formation of excitons that have principal quantum numbers as large as $n = 25$, provoke a new situation in condensed matter optics. Many problems, such as the light-matter interaction when the excitons with such large quantum numbers are present, will require a new description. Excitonic spectra of highly excited Rydberg excitons observed recently resemble that of a hydrogen atom consisting of a Rydberg series, but even if the hydrogen picture of the exciton seems to be very simple, the calculations with eigenfunctions related to $n = 25$ would be nontrivial. The standard description needs to be revised due to the fact that the size of the exciton is much larger then the wavelength of light used to create it [6]. There are many factors, such as, for example, the band structure, the temperature, the laser power, and the dissipative processes, which should be included in the theoretical description.

Here we neither enter into the analysis of the experiment nor in the calculations of the band structure. We propose a method which gives a simple expression for the optical functions, taking into account excitonic states of arbitrary order, which allows one to obtain theoretical spectra and to analyze the experimental ones. The method is based on the real density matrix approach and uses the Green's function method to solve the Schrödinger-like equations which are typical for this

*david.ziemkiewicz@utp.edu.pl

approach. The method will also give insight into the aspect of polaritons, which are closely related to the excitonic states. The RDMA, initiated by the works by Stahl *et al.* (see, for example, [10,11]), was very successful in describing optical properties of semiconductors for energies near the fundamental gap, where the excitons are relevant. This approach also solved the old ABC problem (for example, [12,13]), at least for the cases with a few excitonic states [11]. In what follows we focus the attention on the optical spectra of Cu_2O. As it follows by the analysis of crystal symmetry, the lines related to odd angular momentum exciton number $\ell = 1,3,..$ are observed [14]. The dominant role is played by the P excitons (the so-called yellow series), but also excitonic states with higher than $\ell = 1$ angular momentum (for example, the F excitons with $\ell = 3$ and H excitons with $\ell = 5$) were observed in the one-photon absorption spectra of high-quality cuprous oxide. Our method gives not only the energy eigenvalues, but also the line shapes of the optical functions, from which we have chosen the susceptibility. The presented theory explains many peculiar characteristics of Rydberg excitons, such as deviations from n^{-3} law of oscillator strengths and n^{-2} law for the excitonic energies, and gives the polariton dispersion relation. Using anisotropic effective masses, we show the energy splitting of the P, F, and H excitons. Our numerical results are in agreement with measurements obtained recently in the outstanding experiments performed by Kazimierczuk *et al.*[7] and Thewes *et al.* [14].

It is believed that the observation of Rydberg excitons allows one to open a new field in condensed matter spectroscopy. For highly excited Rydberg excitons in Cu_2O the scale is over 1 μm [15], so the application of solid-state huge-size excitons as all-optical switching, mesoscopic single-photon devices or their implementation to construct the quantum gates influences the development of new experimental techniques. Additionally, it is interesting to note that the excitonic approach toward the old idea of Rydberg atoms is an example of how the development of one field inspires the others.

Our paper is organized as follows. In Sec. II, we briefly recall the basic equations of the RDMA approach and derive expressions for the interband susceptibility. Next, in Sec. III, the derived expression is analyzed for the case of Cu_2O crystal. In Sec. IV, the derived expression for the susceptibility is used to obtain the polariton dispersion relation of the considered cuprous oxide crystal. In Sec. V we show the impact of the effective-mass anisotropy on the calculated optical properties. In Sec. VI the method of calculating the susceptibility and the polariton dispersion in terms of an appropriate Green's function is presented. In Sec. VII the results for the absorption spectra are presented and discussed. The comparison of obtained results with the experimental data and a brief overview of the optimizing procedure is included. In Sec. VIII we show that the method applied to the case of an indirect gap semiconductor can be used, by appropriate choice of the transition dipole, to investigate the optical properties of direct gap semiconductors. We close with final remarks in Sec. IX.

II. DENSITY MATRIX FORMULATION

Having in mind the experiments by Kazimierczuk *et al.* [7], we will compute the linear optical response of a semiconductor platelet to a plain electromagnetic wave

$$\mathbf{E}_i(z,t) = \mathbf{E}_{i0}\exp(ik_0 z - i\omega t), \quad k_0 = \frac{\omega}{c}, \tag{1}$$

attaining the boundary surface located at the plane $z = 0$. The second boundary is located at the plane $z = L$. As indicated above, we use the RDMA. In the linear case, the optical response is obtained by solving the so-called constitutive equations, supplemented by the Maxwell equations for the wave propagating in the semiconductor crystal. Considering a semiconductor with a nondegenerate conduction band and a λ-fold degenerate valence band, the constitutive equations have the form (for example, [10])

$$\begin{aligned}\dot{Y}(\mathbf{R},\mathbf{r}) = (-i/\hbar)H^{\lambda}_{eh}Y(\mathbf{R},\mathbf{r}) - \Gamma^{\lambda}Y(\mathbf{R},\mathbf{r})\\ + (i/\hbar)\mathbf{E}(\mathbf{R})\mathbf{M}^{\lambda}(\mathbf{r}),\end{aligned} \tag{2}$$

where Y^{λ} is the bilocal coherent electron-hole amplitude (pair wave function), $\mathbf{R}$ is the excitonic center-of-mass coordinate, $\mathbf{r} = \mathbf{r}_e - \mathbf{r}_h$ the relative coordinate, $\mathbf{M}^{\lambda}(\mathbf{r})$ the smeared-out transition dipole density, and $\mathbf{E}(\mathbf{R})$ is the electric field vector of the wave propagating in the crystal. The smeared-out transition dipole density $\mathbf{M}(\mathbf{r})$ is related to the bilocality of the amplitude Y and describes the quantum coherence between the macroscopic electromagnetic field and the interband transitions. Its form depends on the type of the interband transition (direct or indirect gap) and is specified below. The two-band Hamiltonian H_{eh} is taken in the form

$$\begin{aligned}H^{\lambda}_{eh} &= H^{\lambda}_{c.m} + H^{\lambda}_{r},\\ H^{\lambda}_{c.m} &= (-\hbar^2/2)\nabla_R(\underline{\underline{M}}^{\lambda})^{-1}\nabla_R + \hbar\omega^{\lambda}_{g},\\ H_r &= (-\hbar^2/2)\nabla_r(\underline{\underline{\mu}}^{\lambda})^{-1}\nabla_r + V_{eh}(r),\end{aligned} \tag{3}$$

$\underline{\underline{\mu}}^{\lambda}, \underline{\underline{M}}^{\lambda}$ being the exciton-reduced and total mass tensors, respectively, and $\hbar\omega^{\lambda}_{g}$ is the energy gap for the considered pair of energy levels. Operators Γ^{λ} stand for irreversible processes. The coherent amplitudes Y^{λ} define the excitonic counterpart of the polarization,

$$\mathbf{P}(\mathbf{R}) = 2\sum_{\lambda}\int d^3r \mathrm{Re}[\mathbf{M}^{\lambda}(r)Y^{\lambda}(\mathbf{R},\mathbf{r})], \tag{4}$$

which is then used in the Maxwell field equation,

$$c^2\nabla^2_R\mathbf{E} - \underline{\underline{\epsilon}}_b\ddot{\mathbf{E}}(\mathbf{R}) = \frac{1}{\epsilon_0}\ddot{\mathbf{P}}(\mathbf{R}), \tag{5}$$

with the use of the bulk dielectric tensor $\underline{\underline{\epsilon}}_b$ and the vacuum dielectric constant ϵ_0. Having the polarization, we can compute the excitonic susceptibility $\underline{\underline{\chi}}(\omega,k)$,

$$\mathbf{P}(\omega,\mathbf{k}) = \epsilon_0\underline{\underline{\chi}}(\omega,k)\mathbf{E}(\omega,\mathbf{k}). \tag{6}$$

In the present paper we solve Eqs. (2)–(6) with the aim to compute the optical functions (reflectivity, transmission, and absorption) for the case of Cu_2O. The first step is to calculate the dielectric susceptibility. This can be achieved in two ways: (1) by expanding the coherent amplitudes Y^{λ} in terms of eigenfunctions of the Hamiltonian H_r of the relative electron-hole motion, and (2) using the appropriate Green function of the left-hand-side operator in Eq. (2). We begin with method 1

for the case of an unbounded semiconductor crystal. Assume that there exists an orthonormal basis $\{\varphi_n^\lambda\}$ of eigenfunctions of the operator H_r^λ and E_n^λ are the corresponding eigenvalues. The eigenfunctions of the total Hamiltonian H_{eh}^λ have the form

$$\Phi_{\mathbf{k},n}^\lambda = \exp(i\mathbf{kR})\varphi_n^\lambda, \tag{7}$$

with the corresponding eigenvalues

$$\hbar\Omega_n^\lambda(\mathbf{k}) = \sum_{\alpha=1}^{3}\frac{\hbar k_\alpha^2}{2m_\alpha^\lambda} + \hbar\omega_g^\lambda + E_n^\lambda, \tag{8}$$

with the assumption that the total effective-mass tensor has a diagonal form. We also assume that the $\Phi_{\mathbf{k},n}^\lambda$ are eigenfunctions of the damping operators Γ^λ corresponding to the eigenvalues $\gamma_n^\lambda(\mathbf{k})$. Expanding both Y^λ and $\mathbf{M}^\lambda(\mathbf{r})\mathbf{E}(\mathbf{R})$ in terms of $\Phi_{\mathbf{k},n}^\lambda$ and going over to the Fourier representation, we obtain ([16])

$$\chi(\omega,\mathbf{k}) = \frac{1}{\epsilon_0\hbar}\sum_\lambda\sum_n\left[\frac{c_{n\alpha}^{*\lambda}c_{n\beta}^\lambda}{\Omega_n^\lambda(\mathbf{k}) - \left(\omega + i\gamma_n^\lambda(\mathbf{k})\right)} + \frac{c_{n\alpha}^\lambda c_{n\beta}^{*\lambda}}{\Omega_n^\lambda(\mathbf{k}) + \left(\omega + i\gamma_n^\lambda(\mathbf{k})\right)}\right], \tag{9}$$

where

$$\mathbf{c}_n^\lambda = \langle\varphi_n^\lambda|\mathbf{M}\rangle = \int d^3r\ \varphi_n^{*\lambda}(r)\mathbf{M}^\lambda(r). \tag{10}$$

III. THE INTERBAND SUSCEPTIBILITY FOR Cu_2O

We consider the interband transition between the highest valence band (Γ_7^+) and the lowest conduction band (Γ_6^+) in Cu_2O. The conduction band and the valence bands have the same parity and the dipole moment between them vanishes. The $n \neq 1$ line corresponds to excitons with the relative angular momentum $\ell = 1$, and for this reason the absorption process is dipole allowed. To compute the susceptibility, we use the formula (6). For the sake of simplicity, we consider here the case of an isotropic effective electron and hole masses. The anisotropic case will be considered below. The eigenfunctions φ_n are the hydrogenlike atom eigenfunctions,

$$\varphi_n(r) \to \varphi_{n\ell m}(r) = R_{n\ell}(r)Y_{\ell m}(\theta,\phi), \tag{11}$$

where

$$R_{n\ell}(r) = C_{n\ell}\left(\frac{2r}{na^*}\right)^\ell \times M\left(-n+\ell+1, 2\ell+2, \frac{2r}{na^*}\right)\exp-\frac{r}{na^*}, \tag{12}$$

in terms of the Kummer function $M(a,b,z)$ with the normalization

$$C_{n\ell} = \frac{1}{(2\ell+1)!}\left[\frac{(n+\ell)!}{2n(n-\ell-1)!}\right]^{1/2}\left(\frac{2}{na^*}\right)^{3/2}, \tag{13}$$

and with the energies

$$E_n = -\frac{R^*}{n^2}, \quad n = 2,3,\ldots, \tag{14}$$

R^* being the effective excitonic Rydberg energy

$$R^* = \frac{\mu e^4}{2(4\pi\epsilon_0\epsilon_b)^2\hbar^2}, \tag{15}$$

and ϵ_b the bulk dielectric constant. We start with P excitons and assume for $\mathbf{M}(\mathbf{r})$ the following form, appropriate for the indirect gap (for the derivation, see Appendix A):

$$\begin{aligned}\mathbf{M}(\mathbf{r}) &= \mathbf{e}_r\, M_{10}\frac{r+r_0}{2r^2r_0^2}e^{-r/r_0} = \mathbf{e}_r M(r)\\ &= \mathbf{i}M_{10}\frac{r+r_0}{4ir^2r_0^2}\sqrt{\frac{8\pi}{3}}(Y_{1,-1}-Y_{1,1})e^{r/r_0}\\ &\quad + \mathbf{j}M_{10}\frac{r+r_0}{4r^2r_0^2}\sqrt{\frac{8\pi}{3}}(Y_{1,-1}+Y_{1,1})e^{-r/r_0}\\ &\quad + \mathbf{k}M_{10}\frac{r+r_0}{2r^2r_0^2}\sqrt{\frac{4\pi}{3}}Y_{10}e^{-r/r_0},\end{aligned} \tag{16}$$

where r_0 is the so-called coherence radius [10,11]

$$r_0^{-1} = \sqrt{\frac{2\mu}{E_g}}\hbar^2, \tag{17}$$

E_g the fundamental gap, and μ the reduced effective mass for the pair electron-hole. The above expression gives the coherence radius in terms of effective band parameters, but we find it convenient to treat the coherence radii as free parameters which can be determined by fitting the experimental spectra. Mostly one takes it as a fraction of the respective excitonic Bohr radius. Taking into account the $\ell = 1$ states and the $\mathbf{k}$ component of the dipole density (16) and restricting the consideration to the resonant states, we obtain from (9) the P-exciton counterpart of the susceptibility:

$$\chi_P(\omega,\mathbf{k}) = \frac{2}{\epsilon_0\hbar}\sum_{n=2}^{N}\frac{b_{n1}}{\Omega_n(\mathbf{k}) - (\omega + i\gamma_n(k))}, \tag{18}$$

$$b_{n1} = \frac{8\pi}{3}\left(\int_0^\infty dr r^2 R_{n1}(r)M(r)\right)^2, \tag{19}$$

where R_{n1} are the p-symmetric radial hydrogen atom eigenfunctions [see (12) for $\ell = 1$]

$$R_{n1}(r) = C_{n1}\left(\frac{2r}{na^*}\right)M\left(-n+2,4,\frac{2r}{a^*n}\right) \times \exp\left(-\frac{r}{na^*}\right), \tag{20}$$

with the normalization

$$C_{n1} = \frac{1}{3!}\left[\frac{(n+1)!}{2n(n-2)!}\right]^{1/2}\left(\frac{2}{na^*}\right)^{3/2}, \tag{21}$$

where the excitonic Bohr radius a^* is used,

$$a^* = \frac{(4\pi\epsilon_0\epsilon_b)\hbar^2}{\mu e^2}. \tag{22}$$

After performing the calculations (see Appendix B) we obtain the coefficients b_{n1} in the form

$$b_{n1} = M_{10}^2\frac{n^2-1}{n^5}\frac{16\pi}{3}\left(\frac{a^*}{r_0}\right)^4\frac{1}{a^{*3}}\left(\frac{nr_0}{r_0+na^*}\right)^6. \tag{23}$$

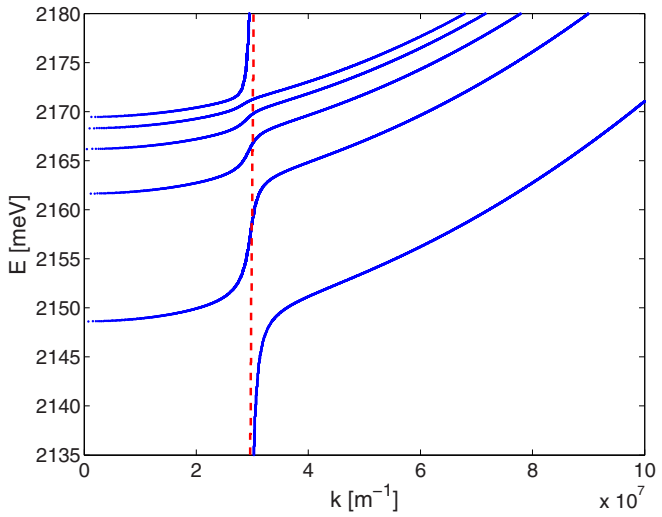

FIG. 1. The polariton dispersion for a Cu_2O crystal, calculated by Eq. (26), taking into account the five lowest excitonic states.

IV. POLARITON DISPERSION RELATION

Having the coefficients b_{n1} and thus the P-exciton part of the susceptibility, we obtain from (5) the polariton dispersion relation

$$\frac{c^2k^2}{\omega^2} - \epsilon_b = \frac{2}{\epsilon_0\hbar}\sum_{n=2}^{N}\frac{b_{n1}}{\Omega_n(\mathbf{k}) - (\omega + i\gamma_n(k))}. \tag{24}$$

It follows that for $k = 0$ and $\gamma_n = 0$ the right-hand side exhibits resonances located at the transversal frequencies ω_{Tn}. In the case under consideration,

$$\hbar\omega_{Tn} = E_{Tn} = \hbar\omega_g - \frac{R^*}{n^2}, \quad n = 2,3,\ldots. \tag{25}$$

Using the oscillator strengths f_{n1} defined in Appendix B, the polariton dispersion relation takes the form

$$\frac{k^2}{k_0^2} - \epsilon_b = \epsilon_b\sum_{n=2}^{N}\frac{f_{n1}\Delta_{LT}^{(2)}/R^*}{(E_{Tn} - E - i\Gamma)/R^* + (\mu/M)(ka^*)^2}, \tag{26}$$

where $k_0 = \omega/c$. The resulting polariton dispersion shape is displayed in Fig. 1. In the above dispersion relation only P excitons are considered. The relation will be much more complicated when excitons with higher angular momentum number are included, for example, F or H excitons.

V. ANISOTROPY EFFECTS

The main difference between the effective hole and electron masses in Cu_2O is the high anisotropy observed for the hole masses while, as expected by symmetry, the electron value remains practically the same for all directions. The anisotropy in the hole effective masses is evidenced by their very different components in the [100], [110], and [111] directions (see, for example, Refs. [17] and [18]). As was shown by Dasbach *et al.* [19] (see also [20]), the total exciton mass in the [0,0,1] direction equals $3m_0$, whereas the value in the [1,1,0] direction is equal 0.66 (for example, [7]) or 0.558 7 ([14]), see Table I. The effective-mass anisotropy plays an important role in the description of the optical properties of excitons. In the RDMA the anisotropy parameter α is defined, $\alpha = \mu_\parallel/\mu_z$, $\mu_\parallel = \mu[110]$ with μ_z being the electron-hole reduced masses in the respective directions. This parameter is then used in modified expressions for the excitonic eigenfunctions and eigenvalues. Instead of (12) we will use

$$R_{n\ell}(r) = C_\ell(2\lambda r)^\ell \times M\left(\ell + 1 - \frac{\eta_{\ell m}}{\lambda}, 2\ell + 2, 2\lambda r\right)\exp(-\lambda r), \tag{27}$$

with $\lambda = \sqrt{-E}$, C_λ is the normalization factor, and

$$\eta_{\ell m}(\alpha) = \int_0^{2\pi} d\phi \int_0^{\pi} \frac{|Y_{\ell m}|^2 \sin\theta\, d\theta}{\sqrt{\sin^2\theta + \alpha\cos^2\theta}}. \tag{28}$$

TABLE I. Two sets of band parameter values for Cu_2O from Refs. [8] and [14], energies in millielectronvolts, masses in free electron mass m_0, lengths in nanometers, $\gamma_1,\gamma_2,\gamma_3$ are Luttinger parameters (here only γ_1, from Ref. [14]), α is the anisotropy parameter, and energies $|E_{n\ell m}| = \eta_{\ell m}^2 R^*/n^2$, $E_{Tn\ell m}$ are positions of resonances.

Parameter	[8]	[14]
E_g	2172.08	2172.08
m_e	0.99	1.01
γ_1		1.79
$m_h[110] = m_{h\parallel}$	0.66	0.5587[a]
$m_h[001] = m_{hz}$[b]	2.01	1.99
$\mu[110] = \mu_\parallel$	0.396	0.3597[c]
$\mu[001] = \mu_z$	0.663	0.672
$M[110] = M_\parallel$	1.65	1.5687
$M[001] = M_z$	3.0	3.0
$\alpha = \mu_\parallel/\mu_z$	0.597	0.535
η_{00}	1.0669	1.1004
η_{10}	1.496	1.1901
η_{30}	1.408	1.168
η_{50}[d]		1.1172
R^*	95.74	86.981
$\lvert E_{100}\rvert$	108.95	105.32
$\lvert E_{210}\rvert$	53.56	30.80
$\lvert E_{410}\rvert$	13.39	7.70
$\lvert E_{430}\rvert$	11.86	7.4162
$\lvert E_{710}$		2.5247
$\lvert E_{750}\rvert$		2.2162
$\lvert E_{730}$		2.4222
E_{TP410}	2158.69	2164.38
E_{TF430}	2160.22	2164.67
E_{TP710}		2169.56
E_{TF730}		2169.66
E_{TH750}		2169.86
$\Delta E(FP)$	1.53	0.29
a^*	1.00	1.1
ϵ_b	7.5	7.5
ϵ_∞	6.5	6.5

[a] from $m_h = 1/\gamma_1$.
[b] By $M - m_e$ for the total mass $M = 3m_0$ [19].
[c] From $\mu = 1/\gamma_1', \gamma_1' = \gamma_1 + m_0/m_e$.
[d] From $\eta_{\ell m} \approx 1 + \frac{1-\alpha}{2}\frac{(2\ell^2+2\ell-1)}{(2\ell-1)(2\ell+3)}$.

Bound states appear when the index $(\ell + 1 - \eta_{\ell m}/\lambda)$ attains zero or a negative integer, so that the discrete eigenvalues are given by [21,22]

$$n = 1,2,\ldots,$$
$$\ell = 0,1,2,\ldots,n-1,$$
$$E_{n\ell m} = -\frac{\eta^2_{\ell m}(\alpha)R^*}{n^2}, \quad m = 0,1,2,\ldots,\ell. \tag{29}$$

For the lowest eigenvalues we can use another expression,

$$E_{n\ell} = -A^2_{n\ell}R^*, \tag{30}$$

with

$$A_{10} = \frac{2}{1+\sqrt{\alpha}},$$
$$A_{20} = \frac{2(1+2\sqrt{\alpha})}{3(1+\sqrt{\alpha})^2},$$
$$A_{30} = \frac{1}{15}\left\{\left[\frac{2}{1+\sqrt{\alpha}} \times\left(\frac{\sqrt{\alpha}}{1+\sqrt{\alpha}} + 2\frac{\sqrt{\alpha}}{(1+\sqrt{\alpha})^2} + \sqrt{\alpha} + 3\right)\right]\right\} \tag{31}$$

etc., see Ref. [22]. The above formulas can explain the huge, as compared to the Rydberg energy, excitonic binding energy, for which we obtained values of 108.95 meV (105.32 meV), depending on the parameters used, see Table I. This values show the property of the observed exciton binding energy in Cu_2O, which is greater than the corresponding Rydberg energy (see, for example, [23] and, more recently, [24]). We can also calculate the P and F excitons resonances using the values of the parameters η_{10} and η_{30}. By extending the formula (16) by inclusion of higher-order excitons (F, H, ...), we use the expression (A6) from Appendix A. The results show that the F exciton resonances are shifted to the higher energy, compared to the P excitons (see Table I), as was described in Ref. [14]. Using the above results we can extend the expressions for the susceptibility, including the effects of F excitons:

$$\chi = \epsilon_b \sum_{n=2}^{N} \frac{f_{n1}\Delta^{(2)}_{LT}/R^*}{(E_{Tn10} - E - i\Gamma)/R^* + (\mu_\parallel/M)(ka^*)^2} + \epsilon_b \sum_{n=4}^{N} \frac{f_{n3}\Delta^{(2)}_{LT}/R^*}{(E_{Tn30} - E - i\Gamma)/R^* + (\mu_\parallel/M)(ka^*)^2}, \tag{32}$$

where the excitonic resonances are given at the energies

$$E_{Tn10} = -\frac{\eta^2_{10}}{n^2}R^*, \quad n = 2,3,\ldots,$$
$$E_{Tn30} = -\frac{\eta_{30}}{n^2}R^*, \quad n = 4,5,\ldots, \tag{33}$$

and

$$f_{n3} = \frac{(n^2-9)(n^2-4)(n^2-1)}{n^9}f, \tag{34}$$

where we set all remaining constants, including the unknown dipole matrix element M_{03} as the factor f, which can be obtained, for example, by fitting the experimental spectra. In particular, the resonances for the $n = 4$ state will be observed at the energies $E_{T410} = E_g - E_{410} = 2158.6$ meV (P exciton) and $E_{T430} = E_g - E_{430} = 2160$ meV (F exciton). This splitting is qualitatively in agreement with the observation by Thewes *et al.* [14]. The differences can be explained by the fact that in Ref. [14] another set of parameters (Rydberg energy, effective masses) was used, as can be seen in Table I. Using the data of Ref. [14], we obtain practically the same values for the excitonic resonances.

VI. GREEN'S FUNCTION METHOD

The constitutive equation (2) is a nonhomogeneous differential equation, which can be solved by using the appropriate Green's function. For bulk crystals, assuming the harmonic time-space dependence and only one valence → conduction band transition, the Green function of the left-hand side operator in (2) satisfies the equation

$$\left(E_g - \hbar\omega - i\Gamma + \frac{\hbar^2k^2}{2M} - \frac{\hbar^2}{2\mu}\nabla^2 - \frac{e^2}{4\pi\epsilon_0\epsilon_b r}\right)G(\mathbf{r},\mathbf{r}') = \delta(\mathbf{r}-\mathbf{r}'). \tag{35}$$

Using the expansion

$$\delta(\mathbf{r}-\mathbf{r}') = \frac{\delta(r-r')}{r^2}\sum_{\ell=0}^{\infty}\sum_{m=-\ell}^{\ell} Y^*_{\ell m}(\theta',\phi')Y_{\ell m}(\theta,\phi), \tag{36}$$

where $Y_{\ell m}(\theta,\phi)$ are spherical harmonics, we look for the Green function in the form

$$G(\mathbf{r},\mathbf{r}') = \sum_{\ell=0}^{\infty}\sum_{m=-\ell}^{\ell} Y^*_{\ell m}(\theta',\phi')Y_{\ell m}(\theta,\phi)g_{\ell m}(r,r'). \tag{37}$$

The functions $g_{\ell m}$ satisfy the equations

$$\left(\frac{d^2}{dr^2} + \frac{2}{r}\frac{d}{dr} + \frac{2}{r} - \frac{\ell(\ell+1)}{r^2} - \kappa^2\right)g_{\ell m} = -\frac{2\mu}{\hbar^2 a^*}\frac{\delta(r-r')}{r^2}, \tag{38}$$

where r is scaled in the excitonic Bohr radii (22) and

$$\kappa^2 = \frac{2\mu}{\hbar^2}a^{*2}(E_g - \hbar\omega - i\Gamma) + \frac{\mu}{M}(ka^*)^2. \tag{39}$$

The solution of (38) is given in the form (for example, [10])

$$g_{\ell m}(r,r') = C(4\kappa^2 rr')^\ell e^{-\kappa(r+r')} \times M(a_\ell,b_\ell,2\kappa r^<)U(a_\ell,b_\ell,2\kappa r^>), \tag{40}$$

where $r^< = \min(r,r')$, $r^> = \max(r,r')$,

$$C = \frac{2\mu}{\hbar^2 a^*}\frac{2\kappa\Gamma(a_\ell)}{\Gamma(b_\ell)}, \quad \begin{matrix} a_\ell = \ell + 1 - \frac{1}{\kappa} \\ b_\ell = 2\ell + 2, \end{matrix} \tag{41}$$

$M(a,b,c)$, $U(a,b,c)$ are *Kummer* functions (confluent hypergeometric functions) in the notation of Abramowitz and Stegun [25], $Y_{\ell m}$ are spherical harmonics, $\Gamma(z)$ is the Euler Γ function, and a^* is the effective excitonic Bohr radius (22). Having the Green function, we calculate the coherent amplitudes,

$$Y(\mathbf{R},\mathbf{r}) = \mathbf{E}(\mathbf{R})\int d^3r'\mathbf{M}(\mathbf{r}')G(\mathbf{r},\mathbf{r}'), \tag{42}$$

and thus the excitonic polarization from Eq. (4),

$$\mathbf{P}(\mathbf{R}) = 2\iint d^3r d^3r' \mathbf{M}(\mathbf{r}) G(\mathbf{r},\mathbf{r}') \mathbf{M}(\mathbf{r}') \cdot \mathbf{E}(\mathbf{R}). \quad (43)$$

The linear dielectric susceptibility tensor

$$\epsilon_0 \underline{\underline{\chi}}(\omega,k) = 2\iint d^3r d^3r' \mathbf{M}(\mathbf{r}) G(\mathbf{r},\mathbf{r}') \mathbf{M}(\mathbf{r}') \quad (44)$$

relates the electric field vector $\mathbf{E}$ to the polarization vector $\mathbf{P}$, and specific polarization components can be considered. From the above Green function expressions, (42), (43), and (44) can be computed once an appropriate expression for $\mathbf{M}(\mathbf{r})$ is considered. Below the gap the imaginary part of the susceptibility $\chi(\omega,k)$ shows maxima in correspondence to the excitonic energy resonances. They are obtained from the singularities in the Green functions $g_{\ell m}$ and for $k = 0, \Gamma = 0$ are given by

$$E_{Tn} = E_g + E_n,$$
$$E_n = -\frac{R^*}{n^2}, \quad n = 1,2,\ldots. \quad (45)$$

To simplify the calculations, we will use the transition dipole intensity in the form [10]

$$\mathbf{M}(\mathbf{r}) = \mathbf{M}_{10} \frac{\mathbf{r}}{r_0^3} \delta(r - r_0). \quad (46)$$

By using the z component given by Eq. (16) and taking into account the orthogonal properties of harmonic functions, we arrive at the following form of the susceptibility tensor element χ_{zz}:

$$\begin{aligned}\chi_{zz}(\omega,k) &= \frac{2}{\epsilon_0}\iint d^3r d^3r' M_z(\mathbf{r}) G(\mathbf{r},\mathbf{r}') M_z(\mathbf{r}') \\ &= \frac{2}{\epsilon_0}\iint d^3r d^3r' M_z(\mathbf{r}) \\ &\quad \times \sum_{\ell=0}^{\infty} \sum_{m=-\ell}^{\ell} Y^*_{\ell m}(\theta',\phi') Y_{\ell m}(\theta,\phi) g_{\ell m}(r,r') M_z(\mathbf{r}') \\ &= \left(\frac{4\pi^2}{3}\right)\left(\frac{2\mu}{\hbar^2}\epsilon_b \frac{2M_{10}^2}{\epsilon_0 \epsilon_b \pi a^*}\right) g_{10}(r_0,r_0) \quad (47)\end{aligned}$$

with

$$g_{10}(r_0,r_0) = \frac{\kappa\Gamma(a_1)}{3}(4\kappa^2 r_0^2) e^{-2\kappa r_0} \times M(a_1,4,2\kappa r_0) U(a_1,4,2\kappa r_0) \quad (48)$$

where $a_1 = 2 - \frac{1}{\kappa}$, r_0 is expressed in the units of a^*, and (39) is used in the form

$$\kappa^2 = \frac{E_g - \hbar\omega - i\Gamma}{R^*} + \frac{\mu}{M}(ka^*)^2. \quad (49)$$

In a similar way we can calculate the excitons of higher-order excitonic states (F,H...). Having the susceptibility tensor elements obtained in terms of the Green function, we can alternatively compute the bulk absorption (in the limit $k \to 0$) and the polariton dispersion. The expressions for the susceptibility in the compact form (47) and as the sum of oscillators, for example (18), are equivalent. The poles in the Green's function correspond to the excitonic resonances given explicitly by Eqs. (29) [or (25) for the isotropic effective masses]. The expression involving the Green's function is more general in such sense that it includes not only all discrete states (and not only a finite number) but also the continuum.

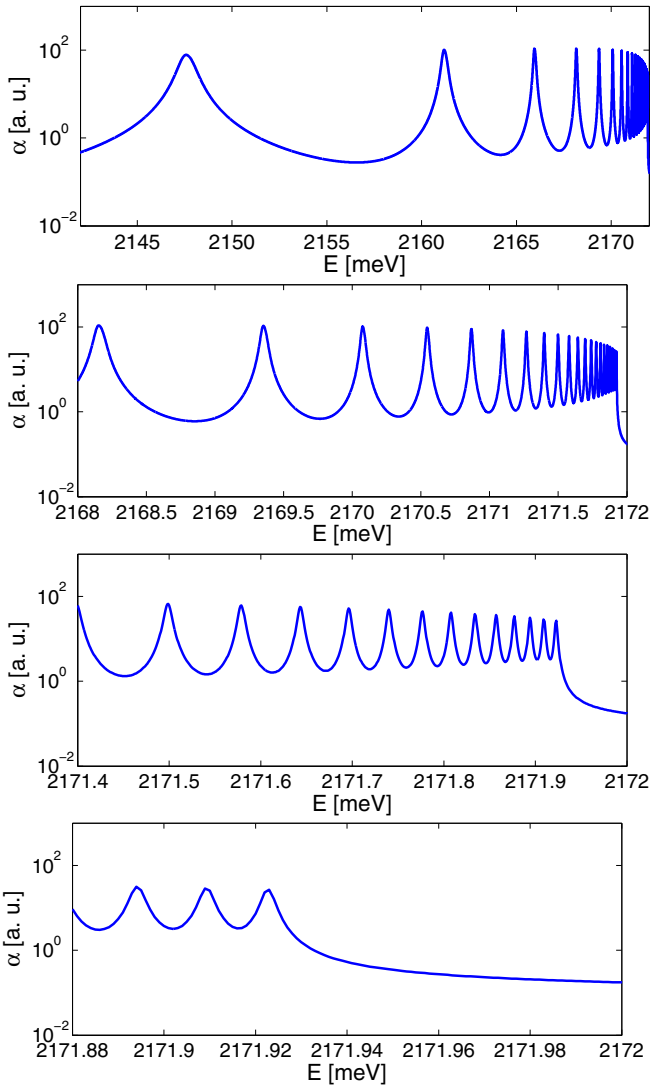

FIG. 2. The bulk absorption of a Cu_2O crystal calculated by Eq. (50) for four energy intervals below the fundamental gap. The logarithmic scale is applied.

VII. RESULTS OF SPECIFIC CALCULATIONS FOR Cu_2O

We performed calculations for the Cu_2O crystal having in mind the experiments by Kazimierczuk *et al.* [7]. The parameters used in calculations are collected in Table I, where a Rydberg energy of 95.74 meV and an effective excitonic Bohr radius of $a^* = 1.00$ nm result from [15] and [22]. First we calculated the polariton dispersion relation, shown in Fig. 1. We observe a multiplicity of values of the wave vectors, which means a multiplicity of polariton waves, much greater than those observed in other semiconductors such as GaAs, for example. This fact should certainly be regarded by computing optical functions such as reflectivity, for example, where the polaritonic aspect is relevant. Then we computed the absorption, shown in Fig. 2. Since the absorption peaks decrease quite rapidly, we applied the logarithmic scale. When the excitonic contributions of F and H are included,

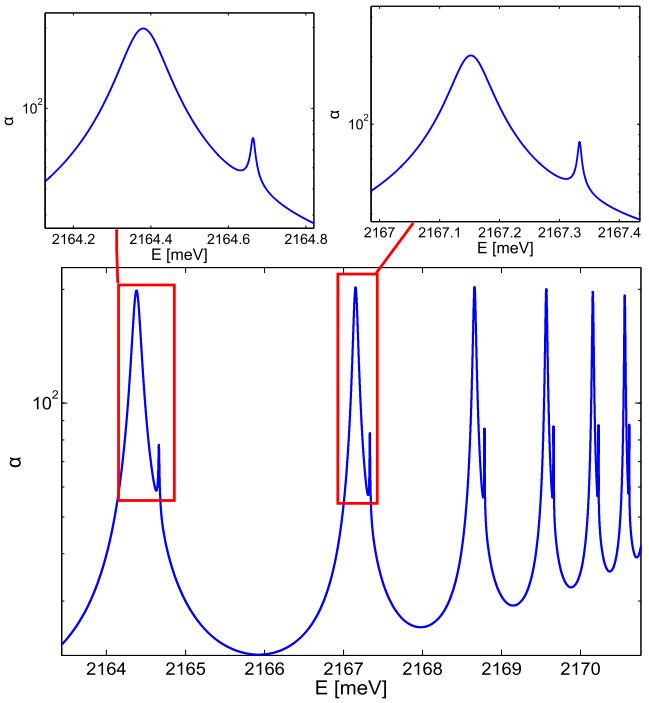

FIG. 3. The absorption spectra, including the effect of P and F excitons, calculated using the parameters from Ref. [14] (see Table I).

we observe the occurrence of additional absorption peaks, as shown in Fig. 3. By the relation (C6) we can establish the dependence between the oscillator forces f_{n1} and the corresponding state number n. The oscillator forces decrease with the number n, but the slope also depends on the coherence radius r_0. The general dependence is shown in Fig. 4, and in Fig. 5 we display the dependence on the coherence radius r_0. As can be seen, the relation $f_n \propto n^{-3}$ is obtained only in the limit $r_0 \to 0$. The best fit to the experimental spectra is obtained for $n^{-2.87}$, as shown in Fig. 4.

In Fig. 5 we present the dependence of the absorption line shape on the magnitude of the coherence radius r_0.

In the case of semiconductors with large excitonic Bohr radii a^* (large compared to the lattice constant, for example, in GaAs), the coherence radius was taken as a small fraction of a^*. In the case of Cu_2O the Bohr radius is not very large (about twice) compared to the lattice constant. Therefore also r_0 cannot be very small. We can take, for example, $r_0 = 0.5a^*$ but the exact value will be estimated by fitting the experimental spectra. As reported in Ref. [26], the longitudinal-transversal energy in Cu_2O is of the order of a few microelectronvolts. We put $\Delta_{LT}^{(2)} = 10\ \mu$eV. Using Eq. (26) and taking into account the lowest 25 excitonic states, we can determine the absorption coefficient from the relation

$$\alpha = \sqrt{\epsilon_b}\mathrm{Im}\left[1 + \sum_{n=2}^{25} \frac{f_{n1}\Delta_{LT}^{(2)}}{E_{Tn10} - E - i\Gamma_{n1}} + \sum_{n=4}^{25} \frac{f_{n3}\Delta_{LT}^{(2)}}{E_{Tn30} - E - i\Gamma_{n3}} + \cdots\right]^{1/2}, \qquad (50)$$

where only $m = 0$ states were accounted for.

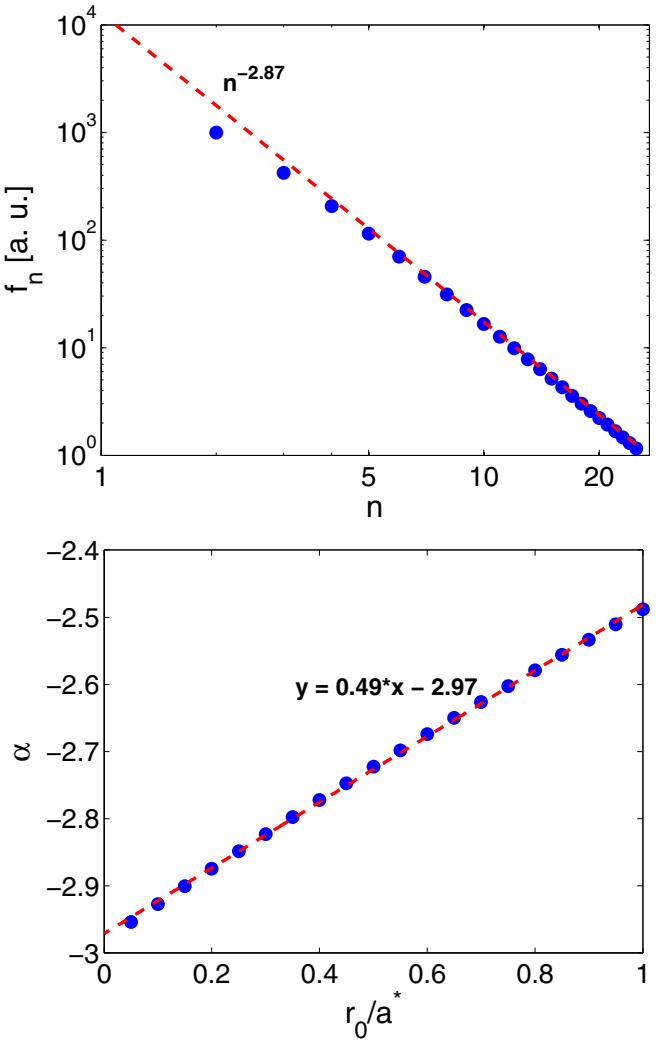

FIG. 4. (a) The dependence of the oscillator forces f_n on the state number n with a linear fit added. (b) The exponent α in the $n^{-\alpha}$ law as a function of the coherence radius r_0.

Recently, we became aware of a new experiment concerning absorption spectra which took into account the probability for absorbing photons from a laser, as well as contributions relating to both coherent and incoherent parts of the spectrum of the excitons by Grünwald *et al.* [27].

VIII. OPTICAL PROPERTIES OF GaN AND ZnO

The method presented above allows one to calculate the optical properties of excitons not only in the case of an indirect gap semiconductor, but also can be applied for the case of direct gap semiconductors. The well-known example of GaAs was extensively studied in the past, also with the help of the RDMA approach. As another example we can consider the direct gap semiconductors GaN and ZnO. They both have some properties similar to Cu_2O considered above. They have wide energy gaps: 3.5 eV for GaN (wurtzite GaN, A- exciton [28]) and 3.44 for ZnO [29]. Their excitonic binding energies are large (28 meV for GaN and around 60 meV for ZnO, Refs. [30] and [31], respectively). They also have

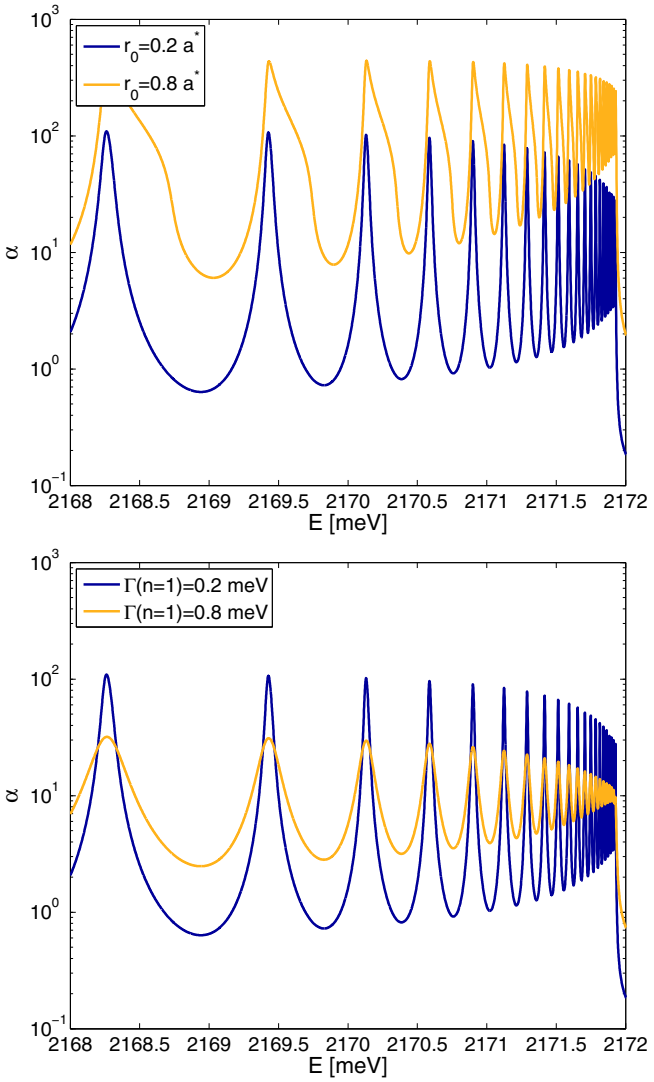

FIG. 5. (a) The dependence of the absorption line shape, calculated for two values of the coherence radius r_0. (b) The dependence on the damping constant Γ.

large dielectric constants and excitons with small Bohr radius. Other parameters such as, for example, effective electron and hole masses, are well known. All those arguments show that the described RDMA approach can be used to calculate the optical properties of GaN and ZnO. Obviously, the specific properties of both semiconductors, such as the dependence of the spectra on the polarization of the incoming wave, and the occurrence of A, B, C excitons, have to be taken into account. These characteristic peculiarities influence the shape of the transition dipole density $\mathbf{M}(\mathbf{r})$, which for the direct transitions has the form (A3), with appropriate definitions of its components depending on the wave polarization [32]. Using (A3) and hydrogenlike wave functions as in (11), we arrive at the susceptibility function in the form

$$\chi = \frac{M_0^2}{\epsilon_0 \hbar} \sum_n \frac{|d_n|^2}{\Omega_n - \omega - i\Gamma_n}, \tag{51}$$

with Ω_n given by (8), and with expansion coefficients [22]

$$|d_n|^2 = \left(\frac{\eta_{00}}{a^*}\right)^3 \frac{n(n - r_0\eta_{00}/a^*)^{2(n-1)}}{\pi(n + r_0\eta_{00}/a^*)^{2(n+1)}}. \tag{52}$$

Similar to the case of Cu_2O, we observe here the dependence on the coherence, which is included in the coherence radius r_0 (17), and the effective-mass anisotropy, represented by the coefficient η_{00} [see also Eq. (28)]. Having the susceptibility we can derive the polariton dispersion, as was done in Sec. IV.

IX. FINAL REMARKS

The main results of our paper can be summarized as follows. We have proposed a procedure based on the RDMA approach that allows one to obtain analytical expressions for the optical functions of semiconductor crystals, including a high number of Rydberg excitons, also for the case of indirect interband transitions. Our results have general character because arbitrary exciton angular momentum number is included. The effect of anisotropic dispersion and coherence of the electron and the hole with the radiation field is outlined. The theoretical findings are confirmed by numerical simulations. We have chosen the example of cuprous dioxide, inspired by the recent experiment by Kazimierczuk *et al.* [7]. We have calculated the absorption spectrum, obtaining a very good agreement between the calculated and the experimentally observed spectra, including the splitting between the P and F excitons. We also obtained a good agreement with the experimental and theoretical results by Thewes *et al.* [14]. Further improvement of the line shape could be achieved with additional correction factors, as presented by Schweiner *et al.* [33]. We have derived the dispersion relation for polariton waves, which differs from the analogous relations for other semiconductors, for example, GaAs. We have also shown that the described method can be used in the case of direct gap semiconductors, indicating the examples of GaN and ZnO. All these interesting features of excitons with high n number which are examined and discussed on the basis on our theory might possibly provide deep insight into the nature of Rydberg excitons in solids and provoke their application to design all-optical flexible switchers and future implementation in quantum information processing.

ACKNOWLEDGMENTS

The authors ave very indebted to M. A. Semina and M. M. Glazov for their remarks and valuable discussion.

APPENDIX A: DERIVATION OF THE TRANSITION DIPOLE DENSITY

In the real density matrix approach the coupling between the band edge and the radiation field is described by a smeared-out transition dipole density $\mathbf{M}(\mathbf{r})$, $\mathbf{r}$ being the relative electron-hole distance. For the transition between the subbands ν_1, ν_2 the definition is [10] with the momentum operator $\mathbf{p}_\rho(\mathbf{k})$,

$$\mathbf{M}^{\nu_1\nu_2}(\mathbf{r}) = \mathbf{M}_\rho(\mathbf{r}) = \int_{1.\mathrm{BZ}} d^3k \tilde{M}_\rho(\mathbf{k}) e^{i\mathbf{kr}}$$
$$= \frac{1}{(2\pi)^3} \frac{ie\hbar}{m_0} \int_{1.\mathrm{BZ}} d^3k \frac{\mathbf{p}_\rho e^{i\mathbf{kr}}}{E_c(\mathbf{k}) - E_{v\rho}(\mathbf{k})}. \tag{A1}$$

For allowed interband transitions we assume that $\mathbf{p}(\mathbf{k}) \approx \mathbf{p}(0)$ and that the interband energy is parabolic in relevant parts of $\mathbf{k}$ space:

$$E_c(\mathbf{k}) - E_v(\mathbf{k}) = E_g + \frac{\hbar^2 k^2}{2\mu}. \tag{A2}$$

Extending the integration to the entire $\mathbf{k}$ space one obtains ([10,34], see also [35])

$$\mathbf{M}(r) = \mathbf{M}_0 \frac{1}{4\pi r_0^2 r} e^{-r/r_0}, \tag{A3}$$

with r_0 defined in Eq. (17). In the case of the forbidden transitions $p(0)$ vanishes. The relevant transition dipole density will be obtained from (A1) by expanding the momentum operator in powers of $\mathbf{k}$. To lowest nonvanishing order in $\mathbf{k}$, we have $\mathbf{p}(\mathbf{k}) \propto \mathbf{k}$. Note that k will arrive in the numerator of (A1) after applying on both sides the operator ∇. So we obtain

$$\mathbf{M}(\mathbf{r}) \propto \nabla \frac{e^{-r/r_0}}{r} = \frac{\mathbf{r}}{r^3 r_0}(r + r_0) e^{-r/r_0}. \tag{A4}$$

Requiring the normalization of the radial part we obtain the formula (16).

In general, the momentum operator $\mathbf{p}_{cv}(\mathbf{k})$ can be expanded in series of k:

$$\mathbf{p}_{cv}(\mathbf{k}) = \mathbf{p}_{cv}(0) + \mathbf{k}[\nabla_k \mathbf{p}_{cv}(\mathbf{k})]_{k=0} + \cdots. \tag{A5}$$

Since we exploited the terms with $\mathbf{p}_{cv}(0)$ and the term $\propto k$, the next terms will be proportional to $\mathbf{p}(\mathbf{k}) \propto \mathbf{k}(\mathbf{k}\cdot\mathbf{k})$, where $\mathbf{k}\cdot\mathbf{k}$ means the dyadic product. Performing, as above, the derivative operation with respect to z (or x, y, respectively) on (A3) and retaining the largest contributions, we obtain (for the sake of exemplification, we present the z component)

$$\begin{aligned}
M_2 \propto \frac{3z^2 - r^2}{r^5} e^{-r/r_0} &= \sqrt{\frac{16\pi}{5}} r_0 \frac{Y_{20}}{r^2} e^{-r/r_0}, \\
M_{3z} \propto \frac{\partial^3}{\partial z^3} &= \frac{3z(3r^2 - 5z^2)}{r^7} e^{-r/r_0} \\
&= -12\sqrt{\frac{\pi}{7}} \frac{Y_{30}}{r^4} e^{-r/r_0}, \\
M_{3x} \propto \frac{\partial^3}{\partial x^3} &= \frac{3x(3r^2 - 5x^2)}{r^7} e^{-r/r_0} \\
&= \frac{1}{r^4}\left[\sqrt{\frac{3\pi}{7}}(Y_{31} - Y_{3-1}) \right. \\
&\quad \left. - \sqrt{\frac{5\pi}{7}}(Y_{33} - Y_{3-3})\right] e^{-r/r_0}, \\
M_{3y} \propto \frac{\partial^3}{\partial y^3} &= \frac{3y(3r^2 - 5y^2)}{r^7} e^{-r/r_0} \\
&= -i\frac{1}{r^4}\left[\sqrt{\frac{3\pi}{7}}(Y_{31} + Y_{3-1}) \right. \\
&\quad \left. - \sqrt{\frac{5\pi}{7}}(Y_{33} + Y_{3-3})\right] e^{-r/r_0},
\end{aligned} \tag{A6}$$

where M_2 corresponds to D excitons, and M_3 to F excitons, M_3 in un-normalized form.

APPENDIX B: THE CALCULATION OF THE COEFFICIENTS b_{n1} AND b_{n3}

First we calculate the coefficients b_{n1} which define the susceptibility related to the P excitons. Using the relations (19), (27), and (13), we obtain

$$\begin{aligned}
C_{n1}^2 \left(\frac{2}{na^*}\right)^2 &= \left(\frac{1}{3!}\right)^2 \frac{(n+1)!}{2n(n-2)!} \left(\frac{2}{na^*}\right)^3 \left(\frac{2}{na^*}\right)^2 \\
&= \frac{4}{9}\frac{n^2 - 1}{n^5}\frac{1}{a^{*5}}.
\end{aligned} \tag{B1}$$

The above expression will be used in the calculation of the coefficients b_{n1}:

$$\begin{aligned}
b_{n1} &= \frac{8\pi}{3}\left(\int_0^\infty dr r^2 R_{n1}(r) M(r)\right)^2 \\
&= \frac{4\pi}{3} M_{10}^2 C_{n1}^2 \left(\frac{2}{na^*}\right)^2 \left[\int_0^\infty dr\, r\, M\left(-n+2,4,\frac{2r}{a^* n}\right)\right. \\
&\quad \left. \times \exp\left(-\frac{r}{na^*}\right)\frac{r + r_0}{r_0^2} e^{-r/r_0}\right]^2 \\
&= \frac{4\pi}{3r_0^2} M_{10}^2 C_{n1}^2 \left(\frac{2}{na^*}\right)^2 \left\{\int_0^\infty dr\, r(r + r_0)\right. \\
&\quad \left. \times M\left(-n+2,4,\frac{2r}{a^* n}\right) \exp\left[-r\left(\frac{1}{na^*} + \frac{1}{r_0}\right)\right]\right\}^2.
\end{aligned}$$

Let us first calculate the integrals involving the confluent hypergeometric function:

$$\begin{aligned}
I &= \int_0^\infty dr\, r(r + r_0)\, M\left(-n+2,4,\frac{2r}{a^* n}\right) \\
&\quad \times \exp\left[-r\left(\frac{1}{na^*} + \frac{1}{r_0}\right)\right] \\
&= \int_0^\infty dr\, r^2\, M\left(-n+2,4,\frac{2r}{a^* n}\right) \exp\left[-r\left(\frac{1}{na^*} + \frac{1}{r_0}\right)\right] \\
&\quad + r_0 \int_0^\infty dr\, r\, M\left(-n+2,4,\frac{2r}{a^* n}\right) \\
&\quad \times \exp\left[-r\left(\frac{1}{na^*} + \frac{1}{r_0}\right)\right].
\end{aligned}$$

The above integrals can be expressed in terms of the hypergeometric function:

$$\begin{aligned}
J_{\alpha\gamma}^{\nu} &= \int_0^\infty e^{-\lambda z} z^{\nu} M(\alpha,\gamma,kz)\, dz \\
&= \Gamma(\nu+1)\lambda^{-\nu-1} F\left(\alpha,\nu+1,\gamma,\frac{k}{\lambda}\right),
\end{aligned} \tag{B2}$$

$F(\alpha,\beta,\gamma,z)$ being the hypergeometric series,

$$F = 1 + \frac{\alpha\beta}{\gamma}\frac{z}{1!} + \frac{\alpha(\alpha+1)\beta(\beta+1)}{\gamma(\gamma+1)}\frac{z^2}{2!} + \cdots. \tag{B3}$$

In the first approximation, assuming that $r_0 \ll na^*$, which is certainly correct for large values of n, we

have

$$I \approx 2\left(\frac{na^*r_0}{r_0+na^*}\right)^3 + r_0\left(\frac{na^*r_0}{r_0+na^*}\right)^2 = \left(\frac{na^*r_0}{r_0+na^*}\right)^2\left[2\frac{na^*r_0}{r_0+na^*}+r_0\right] = r_0(3na^*+r_0)\frac{(na^*r_0)^2}{(r_0+na^*)^3}.$$

Thus

$$b_{n1} = \frac{4}{9}\frac{n^2-1}{n^5}\frac{1}{a^{*5}}\frac{4\pi}{3r_0^4}M_{10}^2\left[3\left(\frac{na^*r_0}{r_0+na^*}\right)^3\right]^2 = M_{10}^2\frac{n^2-1}{n^5}\frac{16\pi}{3}\left(\frac{a^*}{r_0}\right)^4\frac{1}{a^{*3}}\left(\frac{nr_0}{r_0+na^*}\right)^6. \quad \text{(B4)}$$

For the F excitons, taking $\ell = 3$, we have

$$b_{n3} = \frac{144\pi}{7}\left(\int_0^\infty dr r^2 R_{n3}(r)M_3(r)\right)^2 = \frac{144\pi}{7}M_{30}^2C_{n3}^2\left(\frac{2}{na^*}\right)^6 \times\left\{\int_0^\infty dr\, r\, M\left(-n+4,8,\frac{2r}{a^*n}\right) \times\exp\left[-r\left(\frac{1}{na^*}+\frac{1}{r_0}\right)\right]\right\}^2 = \frac{256\times144\times\pi\, r_0^2}{7(7!)^2a^{*9}}M_{30}^2\frac{(n^2-9)(n^2-4)(n^2-1)}{n^9}. \quad \text{(B5)}$$

Roughly speaking, the oscillator strengths related to F excitons also scale as n^{-3} but are of order in magnitudes smaller than those of P excitons, due to the factor $(7!)^2$ in the denominator. In addition, the factor $(n^2-9)(n^2-4)(n^2-1)/n^9$ is smaller than $1/n^3$, as we can see, for example, for $n=4$ (0.015 6 compared to 4.8×10^{-3}). The same holds for the next odd ℓ value (5), where the factor $(11!)^2$ occurs in the denominator of the oscillator strength.

APPENDIX C: ESTIMATION OF THE COHERENCE RADIUS AND THE TRANSITION DIPOLE MATRIX ELEMENTS M_0

The formula (24) allows one to estimate the matrix element M_{10}. Since $k=0$ at a longitudinal frequency ω_L, taking from the right-hand side the main contribution at $n=2$, we have

$$\epsilon_0\epsilon_b\Delta_{LT}^{(2)} = 2b_{21}, \quad \text{(C1)}$$

$$\Delta_{LT}^{(2)} = \hbar\omega_{L2} - \hbar\omega_{T2}, \quad \text{(C2)}$$

$$\Delta_{LT}^{(2)} = \frac{\pi}{\epsilon_0\epsilon_b a^{*3}}M_{10}^2\left(\frac{a^*}{r_0}\right)^4\left(\frac{2r_0}{r_0+2a^*}\right)^6, = (R^*)2\frac{2\mu}{\hbar^2}\frac{M_{01}^2}{\pi\epsilon_0\epsilon_b a^*}f(r_0,a^*), \quad \text{(C3)}$$

with

$$f(r_0,a^*) = \frac{\pi^2}{2}\left(\frac{a^*}{r_0}\right)^4\left(\frac{2r_0}{r_0+2a^*}\right)^6, \quad \text{(C4)}$$

and with regard to the relation $2\mu/\hbar^2 = 1/R^*a^{*2}$. Higher-order coefficients b_{n1} can be expressed in terms of b_{21}:

$$b_{n1} = \frac{32(n^2-1)}{3n^5}\left[\frac{nr_0(r_0+2a^*)}{2r_0(r_0+na^*)}\right]^6,$$

$$b_2 = \frac{16(n^2-1)}{3n^5}\left[\frac{nr_0(r_0+2a^*)}{2r_0(r_0+na^*)}\right]^6,$$

$$\epsilon_0\epsilon_b\Delta_{LT}^{(2)} = \frac{1}{2}f_{n1}\epsilon_0\epsilon_b\Delta_{LT}^{(2)}, \quad \text{(C5)}$$

with

$$f_{n1} = \frac{32(n^2-1)}{3n^5}\left[\frac{nr_0(r_0+2a^*)}{2r_0(r_0+na^*)}\right]^6. \quad \text{(C6)}$$

The higher-order longitudinal-transversal energies $\Delta_{LT}^{(n)} = \hbar\omega_{Ln} - \hbar\omega_{Tn}$ are related to the coefficients b_{n1} by

$$2b_{n1} = \epsilon_0\epsilon_b\Delta_{LT}^{(n)}. \quad \text{(C7)}$$

When $r_0 \ll a^*$, (C5) becomes

$$b_{n1} = \frac{32}{3}\frac{n^2-1}{n^5}b_{21}, \quad \text{(C8)}$$

or, in terms of $\Delta_{LT}^{(2)}$,

$$b_{n1} = \frac{16}{3}\epsilon_0\epsilon_b\frac{n^2-1}{n^5}\Delta_{LT}^{(2)}, \quad n=3,4,\ldots. \quad \text{(C9)}$$

In the above equations and definitions, two parameters are used: the transition dipole matrix element M_{01} and the coherence radius r_0. As it follows from Eq. (C3),

$$\frac{\Delta_{LT}^{(2)}}{R^*} = 2\frac{2\mu}{\hbar^2}\frac{M_{01}^2}{\pi\epsilon_0\epsilon_b a^*}f(r_0,a^*) = 2\frac{M_{01}^2}{\epsilon_0\epsilon_b\pi R^*a^{*3}}f(r_0,a^*), \quad \text{(C10)}$$

the longitudinal-transversal splitting energy and the coherence radius are not independent quantities. Take, for example, the value of the transition dipole matrix element given in Ref. [36] for the $1s\to2p$ transition, in our notation $M_0 = 4.6\,\text{Å} = 1.08\times10^{-28}\,\text{C m}$. Using this value and other parameters for Cu_2O we obtain

$$\frac{\Delta_{LT}^{(2)}}{R^*} = 4.55\,f(r_0,a^*), \quad \text{(C11)}$$

which means that a value of $\Delta_{LT}^{(2)}$ in the order of 1 meV will be obtained for a small (compared to a^*) value of r_0. Thus the situation is the following: either we know the exact value of the LT-splitting energy (as is the case, for example, for GaAs), and the coherence radius can be estimated, or we consider Δ_{LT} and r_0 as two unknown quantities. Then we need two equations to establish them. Such equations can be obtained from the behavior of the dielectric function (here in scalar notation) $\epsilon(\omega)$,

$$\frac{c^2k^2}{\omega^2} = \epsilon(\omega,k) = \epsilon_b + \chi(\omega,k), \quad \text{(C12)}$$

from which we obtain two equations,

$$0 = \epsilon_b + \chi(\omega_L,0), \tag{C13}$$

$$\epsilon_\infty = \epsilon_b + \chi(\omega_g,0) \tag{C14}$$

($\epsilon_\infty = 6.5$ for Cu_2O). From the above relations, which, in turn, also depend on the number of states taken into account, the relation between r_0 and Δ_{LT} can be obtained.

[1] T. F. Gallagher, *Rydberg Atoms, Cambridge Monographs on Atomic, Molecular and Chemical Physics* (Cambridge University Press, Cambridge, UK, 2005).
[2] M. Weidemüller, Nat. Phys. **5**, 91 (2009).
[3] M. Saffman, T. G. Walker, and K. Molmer, Rev. Mod. Phys. **82**, 2313 (2010).
[4] H. Kübler, J. P. Shaffer, T. Baluktsian, R. Löw, and T. Pfau, Nat. Photonics **4**, 112 (2010).
[5] B. T. H. Vercoe, S. Brattke, M. Weidinger, and H. Walther, Nature (London) **403**, 743 (2000).
[6] S. Höfling and A. Kavokin, Nature (London) **514**, 313 (2014).
[7] T. Kazimierczuk, D. Fröhlich, S. Scheel, H. Stolz, and M. Bayer, Nature (London) **514**, 343 (2014).
[8] H. Friedrich and D. Wintgen, Phys. Rep. **183**, 37 (1989).
[9] H. Stolz, R. Schwartz, F. Kiesiling, S. Som, M. Kaupsch, S. Sobkowiak, D. Semkat, N. Naka, T. Koch, and H. Fehske, New J. Phys. **14**, 105007 (2012).
[10] A. Stahl and I. Balslev, *Electrodynamics of the Semiconductor Band Edge* (Springer-Verlag, Berlin, 1987).
[11] G. Czajkowski, F. Bassani, and A. Tredicucci, Phys. Rev. B **54**, 2035 (1996).
[12] J. L. Birman, in *Excitons, Modern Problems in Condensed Matter Sciences*, edited by E. I. Rashba and M. G. Sturge (North-Holland, Amsterdam, 1982), Vol. 2, p. 27.
[13] V. M. Agranovich, *Excitations in Organic Solids* (Oxford University Press, Oxford, UK, 2009).
[14] J. Thewes, J. Heckötter, T. Kazimierczuk, M. Aßmann, D. Fröhlich, M. Bayer, M. A. Semina, and M. M. Glazov, Phys. Rev. Lett. **115**, 027402 (2015).
[15] L. H. G. Tizei, Y.-Ch. Lin, M. Mukai, H. Sawada, A.-Y. Lu, L.-J. Li, K. Kimoto, and K. Suenaga, Phys. Rev. Lett. **114**, 107601 (2015).
[16] G. Czajkowski and W. Chmara, Nuovo Cimento Soc. Ital. Fis., D **9**, 1187 (1987).
[17] W. Y. Ching, Yong-Nian Xu, and K. W. Wong, Phys. Rev. B **40**, 7684 (1989).
[18] E. Ruiz, S. Alvarez, P. Alemany, and R. A. Evarestov, Phys. Rev. B **56**, 7189 (1997).
[19] G. Dasbach, D. Frölich, H. Stolz, R. Klieber, D. Suter, and M. Bayer, Phys. Status Solidi C **2**, 886 (2005).
[20] D. Frölich, J. Brandt, Ch. Sundfort, M. Bayer, and H. Stolz, Phys. Rev. B **84**, 193205 (2011).
[21] G. Czajkowski, F. Bassani, and L. Silvestri, Riv. Nuovo Cimento C **26**, 1 (2003).
[22] F. Bassani, G. Czajkowski, and A. Tredicucci, Z. Phys. B: Condens. Matter **98**, 39 (1995).
[23] G. M. Kavoulakis, Y.-Ch. Chang, and G. Baym, Phys. Rev. B **55**, 7593 (1997).
[24] L. Frazer, K. B. Chang, K. R. Poeppelmeier, and J. B. Ketterson, Phys. Rev. B **89**, 245203 (2014).
[25] M. Abramowitz and I. Stegun, *Handbook of Mathematical Functions* (Dover Publications, New York, 1965).
[26] C. Klingshirn, *Semiconductor Optics*, 2nd ed. (Springer Verlag, Berlin, 2005).
[27] P. Grünwald, M. Aßmann, D. Fröhlich, M. Bayer, H. Stolz, and S. Scheel, arXiv:1511.07742.
[28] B. Monemar, Phys. Rev. B **10**, 676 (1974).
[29] A. Mang, K. Reimann, and S. Rubenacke, Solid State Commun. **94**, 251 (1995).
[30] K. Reimann, M. Steube, D. Frölich, and S. J. Clarke, J. Cryst. Growth **189-190**, 652 (1998).
[31] W. J. Fan, A. P. Abiyasa, S. T. Tan, S. F. Yu, X. W. Sun, J. B. Xia, Y. C. Yeo, M. F. Li, and T. C. Chong, J. Cryst. Growth **287**, 28 (2006).
[32] G. Czajkowski and P. Schillak, Nuovo Cimento Soc. Ital. Fis., D **16**, 213 (1994).
[33] F. Schweiner, J. Main, and G. Wunner, Phys. Rev. B **93**, 085203 (2016).
[34] G. Czajkowski and I. Balslev, Phys. Status Solidi B **130**, 655 (1985).
[35] G. Czajkowski, *Linear Optical Properties of Semiconductor Nanostructures* (UTP University Press, Bydgoszcz, 2006), in Polish.
[36] T. Tayagaki, A. Mysyrowicz, and M. Kuwata-Gonokami, J. Phys. Soc. Jpn. **74**, 1423 (2005).